



INDUCED RADIOACTIVITY OF LDEF MATERIALS AND STRUCTURAL COMPONENTS

B. A. HARMON*, C. E. LAIRD†, G. J. FISHMAN*, T. A. PARNELL*, D. C. CAMP‡, C. E. FREDERICK||, D. L. HURLEY§, D. J. LINDSTROM¶, C. E. MOSS**, R. C. REEDY**, J. H. REEVES††, A. R. SMITH§, W. G. WINN‡‡ and E. V. BENTON|||

*ES84 NASA/Marshall Space Flight Center, Huntsville, AL 35812, †Physics Department, Eastern Kentucky University, Richmond, KY 40475, ‡Nuclear Chemistry Division, L-232, Lawrence Livermore National Laboratory, Livermore, CA 94550, ||Western Area Radiological Laboratory, Tennessee Valley Authority, Muscle Shoals, AL 35660, §Nuclear Science Division, Lawrence Berkeley National Laboratory, MS 72-131, 1 Cyclotron Road, Berkeley, CA 94720, ¶SN4, NASA Johnson Space Center, Houston, TX 77058, **Los Alamos National Laboratory, MS D-436, Los Alamos, NM 87545, ††Battelle Memorial Institute, Pacific Northwest Laboratory, MS P8-08, Richland, WA 99352, ‡‡Westinghouse Savannah River Company, Savannah River Site, Aiken, SC 29808, and |||Physics Research Laboratory, University of San Francisco, San Francisco, CA 94117, U.S.A.

Abstract—We present an overview of the Long Duration Exposure Facility (LDEF) induced activation measurements. The LDEF, which was gravity-gradient stabilized, was exposed to the low Earth orbit (LEO) radiation environment over a 5.8 year period. Retrieved activation samples and structural components from the spacecraft were analyzed with low and ultra-low background HPGe gamma spectrometry at several national facilities. This allowed a very sensitive measurement of long-lived radionuclides produced by proton- and neutron-induced reactions in the time-dependent, non-isotropic LEO environment. A summary of major findings from this study is given that consists of directionally dependent activation, depth profiles, thermal neutron activation, and surface beryllium-7 deposition from the upper atmosphere. We also describe a database of these measurements that has been prepared for use in testing radiation environmental models and spacecraft design. Published by Elsevier Science Ltd

1. INTRODUCTION

The objective of the Long Duration Exposure Facility (LDEF) mission was to investigate the long-term effects of the Earth orbital environment on various materials, systems, and spacecraft components. One measurable effect is the build-up of induced radioactivity caused by bombardment by nuclear particles such as protons and secondary neutrons. The radiation fluxes responsible for the activation are of significant concern to spacecraft designers where manned missions are planned and also in cases where sensitive electronics or detectors are to be flown in space. At least two components of the radiation environment can be sampled passively from analysis of radioactive nuclides formed in proton- and neutron-induced reactions. One is the trapped proton flux encountered in the lower Van Allen radiation belts (mostly the South Atlantic Anomaly) and the other is the high energy cosmic ray flux above the local cutoff rigidity (about 3 GV for the LDEF orbit) (Watts *et al.*, 1989, Kinard and Martin, 1991; Armstrong and Colborn, 1992). In addition, the effect of shielding and the production of secondary particles can also be studied using induced radioactivity though, these require thorough model-

ing of the radiation environment and spacecraft geometry.

Having been in space almost 6 y (2105 d), the LDEF sampled the low Earth orbital environment beginning near solar minimum in 1984 (launch 6 April on Space Shuttle *Challenger*, deployment 8 April at 479 km, 28.5° inclination) and ending at solar maximum in 1990 (retrieval 12 January by Space Shuttle *Columbia* at 319 km, return 20 January). Of the 57 experiments aboard the spacecraft (Clark *et al.*, 1984), some were adversely affected because of the greatly extended mission; however, results from certain radiation-related and astrophysics experiments were actually enhanced. For induced activity studies, the long mission allowed a build-up of radionuclides with relatively small cross sections (~few millibarns (mb)) with half-lives of months to years. The gravity-gradient stabilization and inertial damping system also made the LDEF particularly valuable for radiation studies. The orientation of the spacecraft remained very stable with respect to the flight vector and the center of Earth throughout the mission. From the atomic oxygen experiment A0114 (Peters and Gregory, 1991), it was deduced that there was less than one degree of wobble about any axis of rotation. This remarkably stable configuration

Table 1. Analyzed spacecraft components

Aluminum	Experiment tray clamps and spacer plates, clamp assemblies, end support retainer plate, keel plate, scuff plate spacers, ballast covers, end frame clamps
Titanium	Structural clips
Steel	End frame trunnions, tray clamp screws, and P0004/P0006 canister screws
Lead	Ballast plates
Other materials	Vanadium, nickel, cobalt, tantalum and indium (Exps. M0001, M0002, P0006, and A0114), magnesium, silver, copper, niobium, molybdenum, and germanium (Exps. A0114 and A0171)

allowed sampling of the anisotropic components of the external radiation environment.

This report describes the induced radioactivity analysis of the LDEF performed under the direction of the Ionizing Radiation Special Investigation Group (IRSIG) for NASA. The IRSIG initiated a variety of studies of the radiation environment of LDEF, including induced radioactivity, low-energy electron and proton radiation dosimetry, linear energy transfer spectra, heavy cosmic rays, and radiation damage to materials (Parnell, 1991). A calculative program was also begun to characterize the radiation environment in detail based on the findings of the multidisciplinary approaches to the radiation studies. Calculative support of radiation environmental studies of the LDEF was performed by Science Applications International Corporation (SAIC) (Armstrong *et al.*, 1991, 1993; Armstrong and Colborn, 1993). Other contributions related to

measurements and modeling of the radiation environment can be found in this issue.

The induced radioactivity experimental analysis was a cooperative effort involving eight laboratories, among them two NASA centers: Marshall Space Flight Center (MSFC) and Johnson Space Center (JSC); five DOE laboratories: Lawrence Livermore National Laboratory (LLNL), Lawrence Berkeley Laboratory (LBL), Battelle Pacific Northwest Laboratory (PNL), Los Alamos National Laboratory (LANL), and Westinghouse Savannah River Site (SRS); and the Tennessee Valley Authority (TVA) Western Area Radiological Laboratory. The analysis of the experimental data taken at MSFC was performed at Eastern Kentucky University (EKU). The post-counting assessment of measured specific activities, tabulation of results, and archival effort was performed by EKU and MSFC. The de-integration of experiment trays and disassembly of the

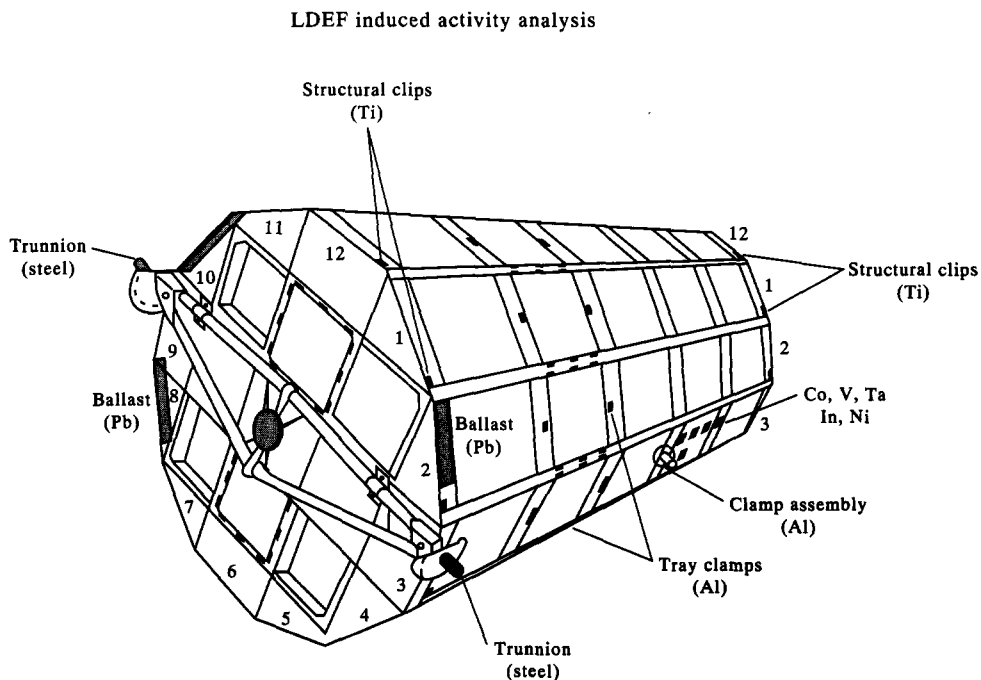


Fig. 1. Components of the LDEF acquired for induced activity analysis. The end support frame/trunnion-mounting structure is on the Earth-facing end of the spacecraft. See Table 2 for a list of components (not all are shown). Row 9 faces the ram direction of the spacecraft.

LDEF spacecraft was performed at Kennedy Space Center. Prior to the removal of any materials, an induced activity study of the entire spacecraft was carried out as a cooperative effort between the U. S. Naval Research Laboratory (NRL), the Institute for Space Science and Technology, and Mississippi State University (Phillips *et al.*, 1991a). The work described in this article refers only to individual sample measurements from the LDEF.

We describe the sample preparation and distribution to the counting laboratories, the analysis procedures, activation results, and a overview of applications of the induced radioactivity data. We discuss the induced activity studies and their relationship to dosimetric and calculated results. Finally, we also describe an archive that has been

prepared for space radiation studies that consists of LDEF gamma ray spectra and specific activities. Some earlier results in preliminary form were reported in Harmon *et al.* (1992); the results presented here supersede those.

2. SAMPLE PREPARATION AND ANALYSIS TECHNIQUES

Materials acquired for analysis of the induced radioactivity are listed in Table 1 and some of their approximate locations on the LDEF are shown in Fig. 1. Some materials were taken from the surface of the spacecraft and consequently were directly exposed to the space environment with minimal

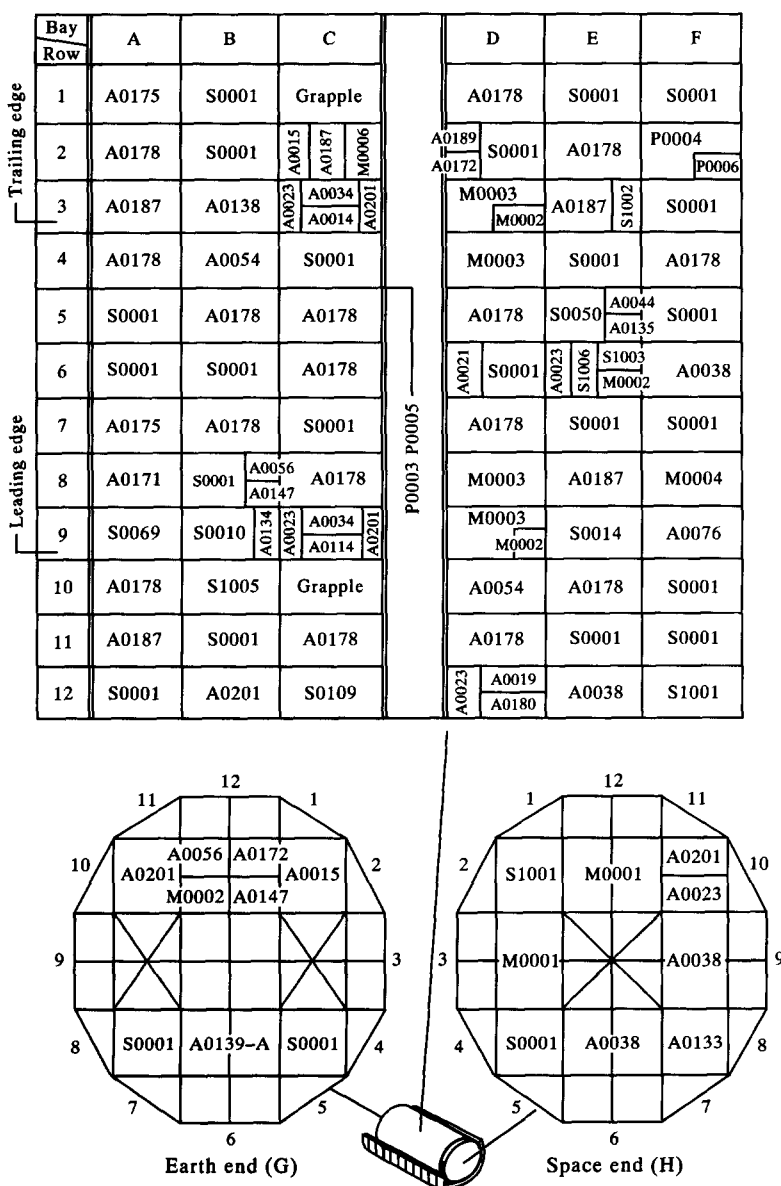


Fig. 2. Experiment tray locations on the LDEF.

shielding; others were at various shielding depths. Approximately 400 samples were assigned to three general categories: (A) the activation sub-experiment (Rich *et al.*, 1984), consisting of metal samples intentionally placed on the spacecraft for activation studies; (B) structural samples from the spacecraft; and (C) materials from other experiments made available for our analysis.

The availability of structural components from category (B) allowed the induced radioactivity to be measured throughout the spacecraft in an organized way. In general, most structural components were not directly suitable for counting in low-level facilities because of their large size and mass. For a complete description of the preparation of the structural samples, processing of other samples received from the LDEF, and details of location and shielding geometry of the samples see Harmon and Laird (1996).

We will refer at times throughout this report to the row-bay and experimental numbering system as designated by the LDEF Project Office (Clark *et al.*, 1984). This system is shown in Fig. 2.

2.0.1. Gamma-ray spectra acquisition. Samples activated aboard LDEF were shipped to the eight participating laboratories to determine the gamma-ray yield from radioactive isotopes found in them. The scientists at each laboratory had the responsibility to provide an appropriate experimental arrangement (usually a heavily shielded high purity germanium detector with the sample placed in close proximity to the detector in a reproducible geometry), count the gamma-ray activity, and correct for detector efficiency and sample self-attenuation. Activity was corrected to 20 January 1990, using known nuclear half-lives. The exception to this was the Be-7 activation, which was decay corrected to 12 January 1990, when the LDEF was stowed in the space shuttle cargo bay. Also, some of the samples were counted at two or more labs for assessment of procedural or other systematic errors. The minimum time between retrieval of the spacecraft, and the beginning of actual counting by laboratories was about 1 month, and although results can be sensitive to many conditions, we were limited to the detection of radioisotopes with rather long half-lives (\approx weeks or greater). V-48, detected in trunnion steel, had the shortest half-life ($T_{1/2} = 16$ d).

Gamma-ray analysis was done with computer codes previously used at each laboratory. These included the codes GAMANAL (Gunnick and Niday, 1972), SAMPO (Routti and Prussin, 1969), and HYPERMET (Phillips and Marlow, 1976). All of these codes fit Gaussian functions with exponential tails and a quadratic background continuum to the photo-peaks found in the spectra. The initial parameters used in these fits were usually determined from spectra of simple calibration sources. Within carefully chosen limits, the codes searched the spectra for peaks and fit the peak function to each peak

found. Multiplets were fit whenever they were found, although most of the LDEF spectra were simple, containing few or no multiplets. Therefore, careful use of even simpler programs such as SPEC-TRAVIEW (SV), prepared at EKU, gave results that agreed with the more sophisticated peak search programs within the statistical accuracy of the data. SV is provided as a tool with the induced activity spectra in the archive (see Appendix).

2.0.2. Corrections for detector efficiency and self absorption. For extended sources like those from the LDEF, where many different sample sizes and shapes must be counted, one of two generic correction procedures was followed. One was to measure the detector efficiency for point sources at various distances along and off the axis extending outward from the center face of the detector. Then, a model was developed to give the efficiency at any chosen point. Another method of making these corrections was completely empirical. Calibration sources from TVA and sets of stainless steel and aluminum absorbers of the same area and thickness range of the LDEF samples were constructed and distributed to the counting laboratories. The planar calibration sources were then counted with various layers of absorbing material between the source and detector. By averaging these count rates in an appropriate fashion, the efficiency and attenuation effects were calculated. Most experimentalists found that both these methods worked well enough to give results within 20%–30% for most LDEF sample measurements. Some systematic errors in excess of 30% were encountered in cases where attenuation corrections were large.

The various counting laboratories were responsible for determining the necessary efficiency-attenuation corrections since they had the most intimate knowledge of their counting systems. LLNL used a procedure incorporated with GAMANAL. This procedure was developed by Gunnick and Niday (1976) and involved a general model of the detector and sample. Included in this model was an effective absorption depth of the photon as a function of depth into the detector.

At SRS a calibration procedure similar to the generic one discussed above was used (Winn, 1992). Point sources were counted at several positions perpendicular to the detector axis at the front face of the detector and through disks and slabs. This gave a set of data at specific perpendicular positions (r) and thicknesses of various materials (h). These results were fit to exponential functions of r and h . After including mass attenuation coefficients, the resultant fit of these data to their model was averaged for the sample to obtain the needed correction. The estimated error in this procedure was 5%.

Analyses of spectral data taken at the LBL's Berkeley Low Background Facility and Oroville Ultra-low Background Facility were similar to the above procedures. A combination of prepared point

sources, distributed sources of assayed U, Th-ores and CP grade potassium chloride, as well as area sources were used. The area sources were thin squares of nickel and copper activated with neutron beams from the LBL 88-Inch Cyclotron to yield nCi and μ Ci activities of Mn-54, Co-56, Co-57, Co-58 and Co-60. Empirical correction factors, merging both the attenuation and geometry parameters, were obtained by using these area sources with stacks of thin metal absorbers (aluminum, cobalt, nickel, tantalum and lead) that encompassed the ranges of thickness encountered with the real samples. Whenever possible, correction factors were generated through the use of the same radionuclides as were measured in actual samples. This strategy facilitated the corrections for gamma cascade summing effects in the high efficiency germanium detectors.

At JSC, LANL and PNL activities were measured through various absorbers of the LDEF sample material using the TVA-prepared sources. Then, a logarithmic average was calculated for the appropriate sample thickness.

The correction for the MSFC data was made using a computer code EFFATN developed at EKU to analyze samples identical to the LDEF samples that had been activated by 200 MeV neutrons at Indiana University Cyclotron Facility (IUCF) (Laird, 1985). The EFFATN algorithm divided the sample into small cells and calculated the efficiency of the detector for each cell and the attenuation through the sample material relative to the efficiency for a point source on the detector axis. A typical number of cells is approximately 32000. This technique was tested originally on data taken on a detector at EKU with a point source measured at 64 evenly spaced positions over the face of the detector and through an absorber similar to the LDEF intentional samples. In the analysis of the samples activated at IUCF, the estimated error in the correction was concluded to be less than 5%.

This procedure was modified slightly with the LDEF activated material. Rather than normalizing the EFFATN correction to a point source, it was normalized to the measured activities of a planar source through layers of stainless steel, aluminum, and plastic of various thickness. Comparisons were also made with results from JSC where efficiencies were obtained by counting the calibration source in front and behind of the nickel samples. Also, the tantalum samples flown aboard LDEF had Lu-173 present. This radioisotope emitted a range of gamma rays from 170 to 1200 keV. The absolute activities calculated with EFFATN agreed to within the 5% assumed accuracy. The resulting specific activities using the EFFATN-deduced efficiencies for activation samples from Experiment A0114 counted at MSFC also agreed well with the results from SRS using Winn's method (see Table 2). Thus, the agreement between the activities measured through the sample material empirically, versus modeling the

attenuation, indicated the validity of the EFFATN corrections.

3. ACTIVATION RESULTS

3.1. Aluminum clamp and spacer plates

The extraction of specific activities from the aluminum experiment tray clamp plates yielded some of the most valuable results from the LDEF. Significant amounts of two radionuclides, Na-22 and Be-7, were observed, and were found to be of different origins. Na-22 was produced as a result of trapped-proton activation and cosmic-ray interactions at higher energies so that we would expect activation by Na-22 throughout the spacecraft. In contrast, the distribution and level of Be-7 activity was a major surprise of the LDEF study (Fishman *et al.*, 1991). The trapped protons, which generate reactions in roughly the 20–120 MeV range, do not make significant amounts of Be-7; it was expected primarily as a spallation product of relatively energetic cosmic ray interactions (cross section ≤ 1 mb for proton energies below 100 MeV (Armstrong and Colborn, 1992)). A large concentration of Be-7 was discovered on the exposed metallic parts on the leading side (i.e., the ram direction) of the LDEF. At approximately the same time, the NRL group, examining 'full' spacecraft results from a large bank of germanium detectors, reported Be-7 unevenly distributed around the spacecraft (Phillips *et al.*, 1991a). A series of tests showed that the isotope was restricted to a thin layer on the surface of the aluminum (Fishman *et al.*, 1991; Gregory *et al.*, 1991), and could only have been produced as a result of atmospheric deposition combined with adsorption to the metallic surfaces caused by spacecraft motion.

Each experiment tray on the LDEF was attached to the main frame of the spacecraft by 6 to 8 of the aluminum (alloy 6061) clamps (see Fig. 1). Most of the tray clamps were of uniform dimensions (1–15/16" wide, 5" long and 0.186" (~3/16") thick). A thinner aluminum spacer plate (15/16" wide or 1–15/16" wide by 4–15/16" long and 0.120" (~1/8") thick) was mounted underneath each tray clamp. The clamp plates and spacers were small enough to be counted without alteration in the low-background facilities. Each clamp/spacer assembly was attached with three steel bolts and washers. The bolts (alloy A286) were counted separately from the aluminum parts.

About 50 clamp plates were counted at the Tennessee Valley Authority (TVA) Western Area Radiological Laboratory. The TVA laboratory had nine germanium detectors in low-background shielded enclosures and were able to count all the samples within a few weeks. This was critical for the Be-7 (half-life 53 d, 478 keV gamma ray) measurements, and also for several longer 70 h counts to map

more subtle trends in the directional character of the Na-22 activity. All clamps were counted with the space-exposed (or outwardly-directed) side of the plates toward the detector. A few were counted with the inward side of the plate toward the detector although no significant gradient could be found by comparing activities between the front and back side measurements.

Several clamp plates were counted at other laboratories to independently verify the TVA calibration procedure. In Table 2, we present measurements from SRS (Winn, 1993) and activities for the same clamp plates counted at TVA. SRS obtained the efficiency for thin samples such as the clamp plates using the point source mapping technique discussed in Section 2.0.2. In addition, because the measurements were made with a high efficiency 90% germanium detector, a summing correction was also required to the peak efficiency for Na-22. The summing correction to the 1275 keV peak efficiency was measured to be 1.72 for the 90% detector. TVA used a 2" × 5" calibration area source to compute a direct average of measurements of the calibration source placed in the front and back of the clamp plate. The lower efficiency germanium detectors at TVA (15%–30%) have a minor summing correction for Na-22. Even though we were limited to only a common sample of 6 plates, comparison of these results showed that the trends were reasonably consistent between the two data sets. The computed differences between measurements also appeared consistent within statistical error.

For presentation of results, the clamp plates from the side rows from LDEF were classified according to bay and row numbers on the LDEF, and then by position number on a particular experiment tray. These designated numbers were converted into an equivalent angle of the clamp as measured from the ram direction (East) of the spacecraft. The clamp plates were mounted along the perimeter of the experiment trays (eight per tray for side trays in rows 1–12) every 15° with respect to the flight vector. Further, a pinhole collimator on the atomic oxygen experiment A0114 (Peters and Gregory, 1991) determined that the spacecraft was yawed 8° from row 9 toward row 8 (clockwise as viewed from the space end of the LDEF). We therefore defined an angle θ counterclockwise around the spacecraft as

viewed from the space end with $\theta = 0^\circ$ corresponding to the ram (East) direction. This angle in degrees, reflecting the 8° clockwise yaw, can be computed from the LDEF row number (row number) and position number for any clamp as

$$\theta = \{(row\ number)*30 + 67 + n*15\} \bmod 360;$$

where $n = 0$ for clamp positions 1, 2 and 3, $n = 1$ for clamp positions 4 and 8, and $n = 2$ for clamp positions 5, 6 and 7. The modulo 360 insures that θ is between 0° and 360°.

The regular placement of the clamps over the entire surface of the spacecraft allowed the activation due to the anisotropic proton fluxes to be mapped. The Na-22 activity (half-life 2.6 y, 1275 keV gamma ray) from the experiment tray clamp plates allowed sampling of flux in a plane aligned with the East, West, North and South directions. The distribution of Na-22 activity on the clamp plates as a function of angle from the leading edge of the spacecraft is shown in Fig. 3. The results indicate a clear peak in the southwest direction for the activation that reflects the maximum in the anisotropic flux of trapped protons (Watts *et al.*, 1989).

Two calculations are shown for comparison in Fig. 3. The first is a one-dimensional (1-D) calculation considering only proton activation along a normal direction to a semi-infinite slab of aluminum. The input spectrum was derived from the proton anisotropy model of Watts *et al.* (1989) normalized to the AP8MIN flux at 450 km (Sawyer and Vette, 1976). The second is a more realistic calculation that incorporated time-dependent trapped proton fluxes (Watts *et al.*, 1993a) and explicitly treated the effects of shielding and secondary particles (Armstrong and Colborn, 1992). The input AP8 fluxes were recently revised to include a finer interpolation of magnetic field data at low altitude (Daly and Evans, 1993). The dominant effect that accounts for the difference in the two models was the treatment of the external fluxes. The altitude of the spacecraft gradually decreased through most of the mission, then more quickly over the final year. This strongly reduced the overall proton fluence over the mission according to the revised model calculations. The models under predict the measured activation by about 30%–50%, depending on the strength of the calculated anisotropy. This apparent underestimation by model calculations of radiation exposure to the LDEF is also indicated from dosimetric studies (Benton *et al.*, 1993). [More details of the LDEF radiation model calculations can be found in this issue (Armstrong *et al.*, 1996; Watts *et al.*, 1996).]

The directional dependence of the Be-7 activity is shown in Fig. 4 for the aluminum clamp plates counted by TVA. The same scheme for plotting the Na-22 activity was used (leading edge at 0°), although the zero point of the horizontal axis has been shifted for clarity away from that of Fig. 3. For the efficiency

Table 2. Comparison of experiment tray clamp plate Na-22 activities

Sample ID	Activity (SRS) (dis/s/kg)	Activity (TVA) (dis/s/kg)	Difference (dis/s/kg)
B7-5	4.61 ± 0.19	4.46 ± 0.38	− 0.15 ± 0.42
D7-2	5.17 ± 0.18	5.83 ± 0.38	+ 0.66 ± 0.42
G6-4	5.34 ± 0.22	6.26 ± 0.81	+ 0.92 ± 0.84
G6-10	3.55 ± 0.18	3.29 ± 0.56	− 0.26 ± 0.59
H6-4	4.80 ± 0.20	4.55 ± 0.64	− 0.25 ± 0.67
H9-12	4.63 ± 0.16	4.76 ± 0.81	+ 0.13 ± 0.82

Table 3. Summary of induced radioactivity sub-experiment measurements

Activation Sample	Product Isotope	Tray H-12 (space end) Exp. M0001	Tray G-12 (Earth end) Exp. M0002	Tray C-9 (leading edge) Exp. A0114	Tray C-3 (trailing edge) Exp. A0114	Tray F-2 (trailing edge) Exp. P0006
Nickel	Sc-46			10.9 ± 3.5 (c)		1.6 ± 0.4 (a)
	Mn-54	36.1 ± 5.4 (c)	27.2 ± 3.9 (c)		66.2 ± 5.8 (c)	37.8 ± 4.4 (c)
		34.7 ± 1.5 (d)	25 ± 3.4 (e)			27 ± 0.9 (a)
	Co-56	31.2 ± 20.0 (c)	35 ± 13.1 (c)		65.7 ± 8.6 (c)	35.3 ± 11.9 (c)
		37.3 ± 2.0 (d)	29 ± 4.8 (e)			33 ± 1.3 (a)
	Co-57	319 ± 16 (c)	225 ± 14.5 (c)		462 ± 26 (c)	222 ± 14 (c)
		201 ± 9.7 (d)	403 ± 35 (e)			322 ± 2(a)
	Co-58	37.4 ± 2.7 (d)	55 ± 9.5 (c)		56.8 ± 8.1(c)	32.2 ± 9.2 (c)
			62 ± 7.3 (e)			42 ± 1.6 (a)
	Co-60	5.1 ± 0.2 (a)	4.7 ± 0.2 (a)		11 ± 4 (c)	4.7 ± 0.3 (a)
	12 ± 7.8 (c)			6.3 ± 0.3 (a)		
	7.6 ± 3.4 (d)					
	9.0 ± 0.9 (g)					
Tantalum	Lu-172	56 ± 2.1 (h)	40 ± 1 (h)		72.2 ± 6.5 (c)	47 ± 1 (h)
		45 ± 2 (b)	39 ± 2 (e)		63 ± 2 (b)	42 ± 2 (b)
			33 ± 2 (b)		75 ± 2 (h)	36 ± 1.1 (a)
	Lu-173	120 ± 9.8 (h)	171 ± 12 (h)		124 ± 26 (c)	91 ± 4 (h)
		167 ± 21 (b)	66 ± 6 (e)		143 ± 5 (h)	161 ± 8.3 (a)
		89 ± 18 (b)		182 ± 17 (b)	141 ± 20 (b)	
Hf-175	38 ± 5.7 (h)	19 ± 2 (h)		27.4 ± 6.4 (c)	25 ± 2 (h)	
			39 ± 2 (h)		37 ± 1.9 (a)	
Ta-182	116 ± 8.1(h)	45 ± 4 (h)		36.7 ± 11.6 (c)	135 ± 4 (h)	
		35 ± 5 (e)		38 ± 2 (h)	90 ± 2.3 (a)	
Vanadium	Sc-46	21 ± 6.0 (b)	16 ± 1.3 (b)	21.1 ± 12.1 (c)		17.4 ± 1.1 (a)
		13 ± 1.7 (g)	16 ± 5.3 (e)	20 ± 1.5 (b)		21 ± 2.7 (b)
		19.8 ± 6.1 (d)		24 ± 2.0 (h)		
Indium	Rh-102	2.2 ± 0.6 (a)	2.3 ± 0.3 (a)	3.2 ± 0.4 (a)		2.2 ± 0.9 (a)
	Ag-110m	3.2 ± 0.8 (a)	2.3 ± 0.3 (a)	3.9 ± 0.5 (a)		5.1 ± 1.0 (a)
	Sn-113	35 ± 4.2 (a)	21 ± 1.2 (a)	25.8 ± 9.7 (c)		54 ± 3.6 (a)
		22 ± 3.8 (e)	41 ± 2.7 (a)			
	In-114m	190 ± 115 (a)	35 ± 15 (a)	55 ± 35 (a)		105 ± 20 (a)
Cobalt	Mn-54	77.2 ± 3.1 (d)	91 ± 3.8 (e)	111 ± 12 (c)		
			62 ± 1.4 (f)	41 ± 1.1 (a)		
			28 ± 1.4 (a)	80.9 ± 1.9 (d)		
	Co-56		22 ± 3.8 (e)	20.4 ± 10.2 (c)		
			9.6 ± 2.5 (d)			
	Co-57	129.2 ± 3.5 (d)	302 ± 5.4 (e)	241 ± 17.1 (c)		
			211 ± 1.6 (f)	125 ± 1.6 (a)		
			83.6 ± 1.7 (a)	141.1 ± 5.5 (d)		
	Co-58	93.7 ± 5.6 (d)	116 ± 20 (e)	95.5 ± 15.7 (c)		
			107.0 ± 5.2 (d)			
Co-60	158.5 ± 3.5 (d)	26.3 ± 2.3 (e)	21.9 ± 0.7 (d)			
	207 ± 10 (g)	23 ± 0.8 (f)	30.2 ± 5.6 (c)			
		31.6 ± 1.7 (g)	18.3 ± 0.5 (a)			
		20.0 ± 0.7 (a)	32.4 ± 1.7 (g)			

(a) LBL (Smith and Hurley, 1991)

(b) SRS (Winn, 1992, 1993)

(c) MSFC/EKU (Laird, 1996)

(d) Batelle PNL (J. Reeves, private comms. 1991, 1992)

(e) LLNL (D. Camp, private comm. 1991)

(f) LBL (A. Smith, private comm. 1993)

(g) Batelle PNL (Reeves *et al.*, 1993)

(h) JSC (private comms. 1991-1993)

determination, instead of a bulk correction for the thickness of the sample, only the front surface was assumed to contain the Be-7 activity. This assumption is consistent with strip and etch tests performed on a thermal isolation plate from Experiment A0114 in tray C-9. These results clearly indicated a peak in the leading direction, opposite to the trend of Na-22. A cosine function was plotted against the results to

illustrate the dependence of the activity on the effective area presented to the ram direction. We see that the data indicated a flatter dependence for the 2-3 leading rows; the reason for this is unknown. This behavior was also seen in the NRL data (Phillips *et al.*, 1991a).

Some results (Fishman *et al.*, 1991) have been reported for the amount of Be-7 activity per unit area

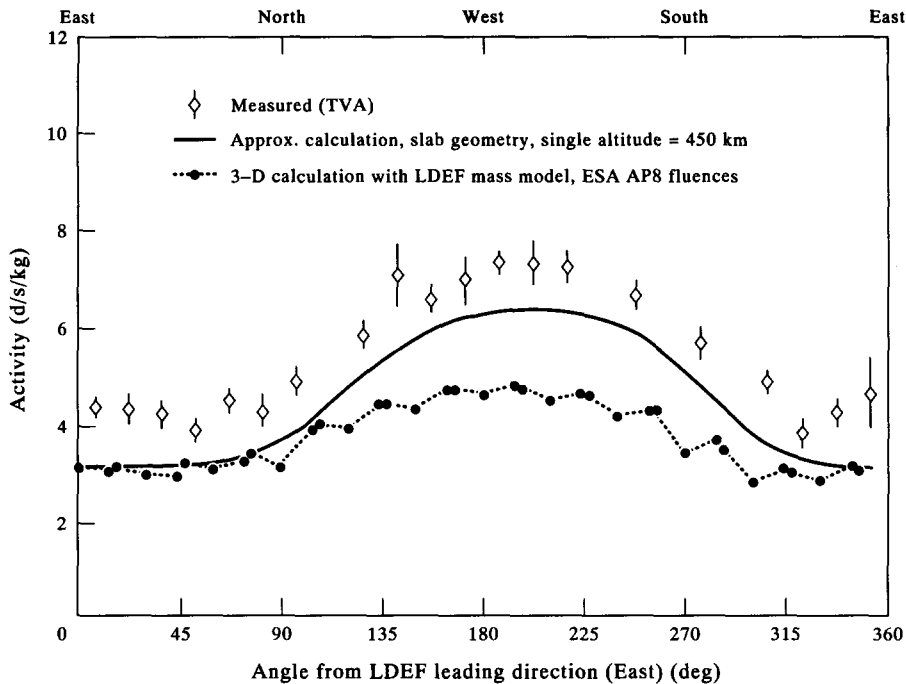


Fig. 3. Na-22 activities in aluminum tray clamps as a function of angle from the leading side of the spacecraft measured from the 1275 keV gamma ray line. Each datum represents a sigma-weighted average of activities for clamps that were mounted at the same angle respect to the flight vector. Two calculations are presented here: (1) A one-dimensional model (no out-of-plane scattering or secondary radiation considered) for induced activation using the Watts model (Watts *et al.*, 1989) for anisotropic trapped proton fluxes, normalized to the AP8MIN (Sawyer and Vette, 1976) flux at 450 km for a semi-infinite slab of aluminum, and (2) a fully three-dimensional treatment incorporating the Watts model, the ESA version of AP8 (Daly and Evans, 1993), as well as adjustments for solar cycle variations and spacecraft altitude. In addition, primary and secondary radiation processes are treated explicitly, coupled with a mass model of the LDEF spacecraft (Armstrong and Colborn, 1993; Watts *et al.*, 1993a). Calculation (2) was performed at specific locations of the clamp plates around the spacecraft. The alternating up-down appearance of the 3-D calculation reflects a regular pattern in the amount of structural support material beneath the clamps, which shields the clamps from flux through the backside of the spacecraft.

on various metal surfaces taken from the leading side of the LDEF. From aluminum and steel materials (the leading side trunnion surface also showed Be-7), the areal density was about 5×10^5 atoms/cm². Assuming the adsorption process is near 100% efficient, it was found that the upper atmospheric concentration of Be-7 was roughly 3.8×10^6 atoms/gram of air, or about three orders of magnitude in excess of that produced by cosmic ray reactions in the denser atmosphere at 20–60 km. It is not yet clear what mechanism transported Be atoms to the upper atmosphere or whether the upper atmospheric concentration of Be-7 was abnormally high near the end of the LDEF mission. The mechanism must be able to transport Be-7 to orbital altitudes on a time scale less than the mean lifetime of Be-7. An explanation based purely on diffusion of free atoms of Be-7 above 100 km has been proposed (Petty, 1991). Increased solar activity in late 1989, just before retrieval of the LDEF, may have been an important factor (Phillips *et al.*, 1991b). The inflow of charged particles from the sun increases the atmospheric temperature and hence the scale height for diffusion.

More details about the experimental and theoretical status of radionuclide production in the upper atmosphere can be found in this issue (Gregory, 1996).

The experiment tray spacer plates, which were mounted beneath the clamp plates, also showed detectable Na-22, mostly on the West side of the LDEF, and no Be-7. These results have not been systematically analyzed, but showed activities of ~2–3 dis/s/kg. The bulk activity of the spacer plates should be lower than that of the clamp plates for a given direction consistent with shielding from the overlying clamp plates.

3.2. Aluminum keel plate, end support retainer plate, and other aluminum components

The keel plate (at the base of the keel trunnion along row 6, North side of LDEF) and the end support retainer plate (both alloy 6061) (see a circular area at the center of the end frame support in Fig. 1) were both cut into samples roughly of 2" × 2" area and 3/8" thick. Samples were individually counted at different laboratories. The distribution of activities for both plates are shown in

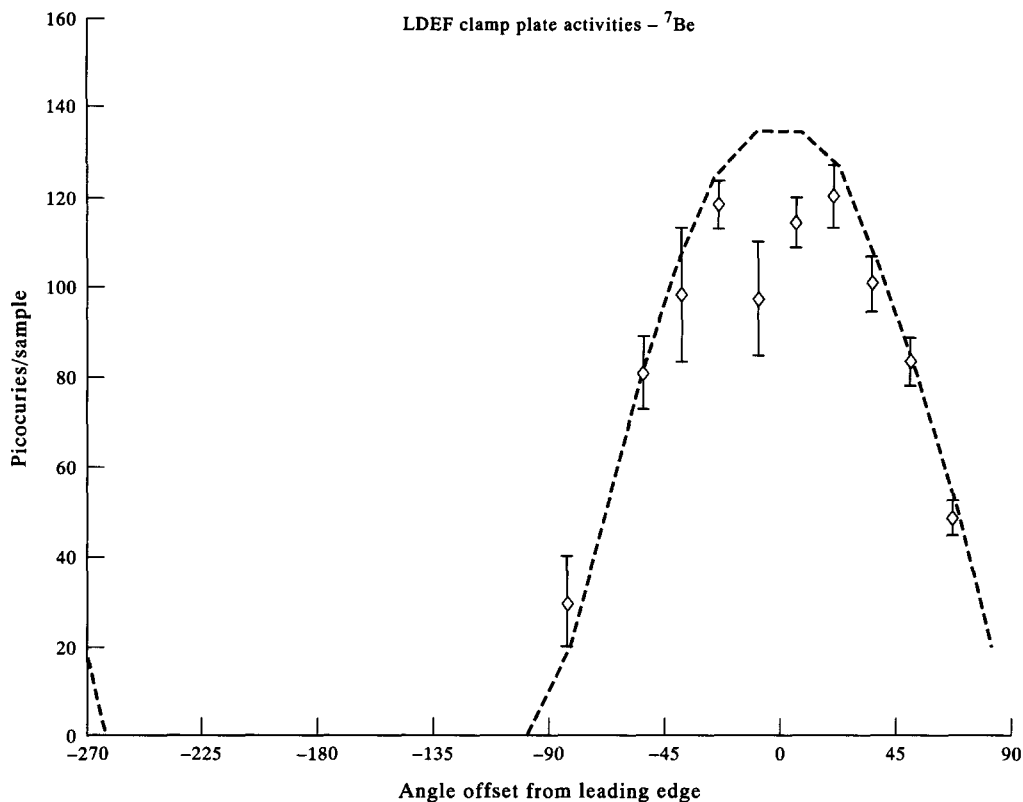


Fig. 4. Be-7 activities measured from the 478 keV gamma ray line in aluminum tray clamps as a function of angle from the leading direction (defined to be 0°). The dashed curve is a cosine function representing the effective surface area exposed to atmospheric beryllium.

Fig. 5 as taken from measurements by LBL (Smith and Hurley, 1991), LANL, JSC and SRS (Winn, 1993). The triangularly-shaped samples KP-2 and KP-5 on the keel plate were counted together as were KP-8 and KP-11.

The keel plate was exposed to the westerly-peaked SAA flux and showed a correspondingly higher activity in KP-2, 3, 4, and 5 on one side of the plate than KP-8, 9, 10, 11 on the opposite side. The retainer plate, which saw flux mainly from the Earth direction, had a much more uniform activation. The activity of the end support retainer plate should be compared to the earth end clamp plate data for G6-4 and G6-10 listed in Table 2.

The clamp assemblies, located behind the main (central) trunnion scuff plates, were the thickest samples of aluminum obtained from LDEF. These were large annular rings surrounding the main trunnions that were cut and analyzed for directional and depth dependence similar to the steel trunnions (see below). Some of the results for clamp assembly layers can be found in Reeves *et al.* (1993) and Harmon and Laird (1996) though, most of the measurements were not reported.

The scuff plate spacers and end frame clamps have also been counted; however, their geometry was too complex to extract specific activities easily. Both

materials contained Na-22 and Be-7 activity. The ballast plate covers were rectangular plates mounted over the lead ballast on each end of LDEF. Some of the cover material was processed into 2" x 2" squares and analyzed, but no activities were reported.

3.3. Intentionally-placed samples (activation sub-experiment in experiments M0001, M0002, P0006, and A0114)

These samples consisted of 2" x 2" square plates (thickness 1/8" to 1/4") of vanadium, indium, cobalt, nickel, and tantalum that were chosen because of their simple isotopic makeup and/or significant long-lived radionuclide production. The stable isotopes of cobalt, tantalum, and indium have large thermal neutron cross sections, allowing some separation of neutron and proton fluxes. Four sets of the metallic plates were prepared at MSFC prior to launch of the LDEF and delivered to the principal investigators of various experiments: A0114 Atomic Oxygen; P0006 Linear Energy Transfer (LET) Spectra; M0001 Heavy Ions in Space; and M0002 Trapped Proton Spectra (Rich *et al.*, 1984). Placement and mounting of the metal samples were by principal investigators, resulting in some samples being placed on exposed surfaces and others in significantly shielded locations. Details of the

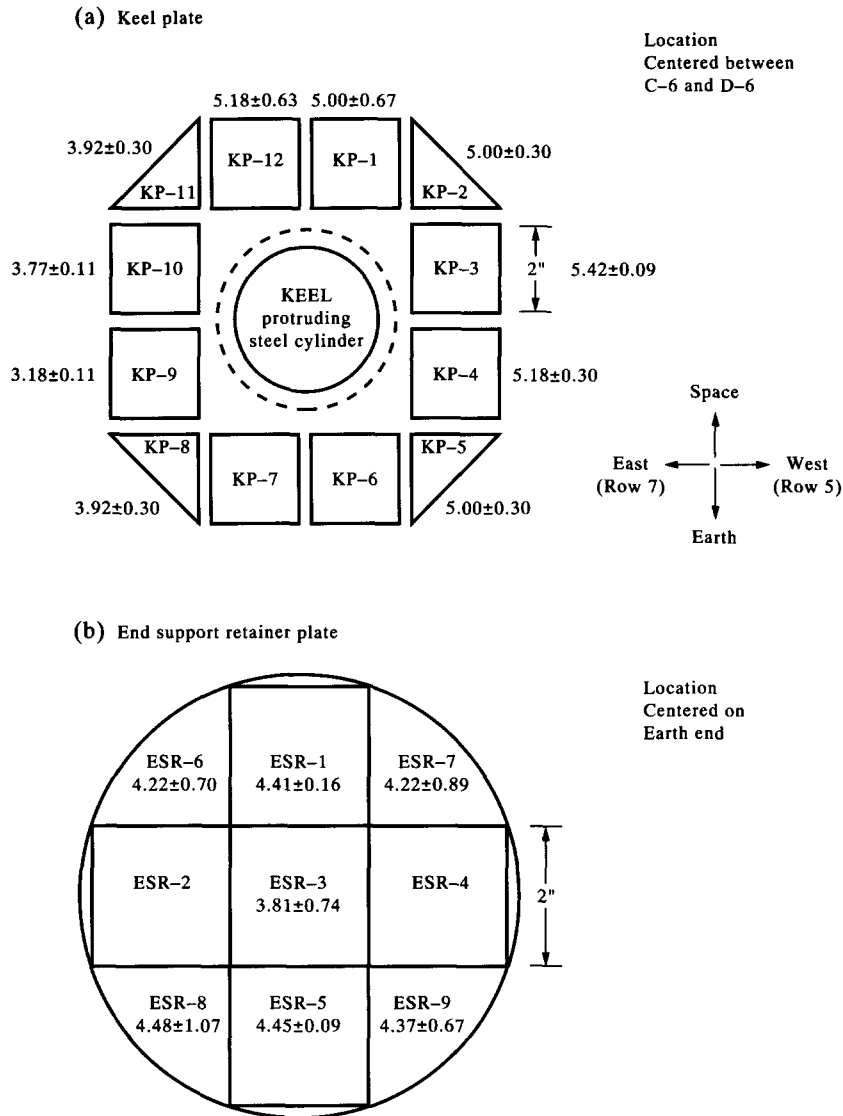


Fig. 5. Na-22 activities (dis/s/kg) in aluminum samples from (a) the keel plate, centrally-located on row 6, and (b) the end support retainer plate on the Earth end of the LDEF. Results from KP-6, KP-7, ESR-2 and ESR-4 were not reported.

intentionally-placed sample geometries can be found in a report to the IRSIG (Harmon and Laird, 1996).

Here we discuss products induced mainly by trapped proton reactions. (We discuss the neutron capture products Co-60, Ta-182 and In-114m in a separate section below.) A compilation of measured sample activities is shown in Table 3. The blank areas of the table for trays C-9 and F-2 indicate the absence of a sample of that particular metal in these trays. Several factors influenced the results: (1) shielding; (2) cross-sections (energy dependent); (3) half-life; and (4) the flux anisotropy, and in the case of the nickel and indium targets, the relative abundance of the target isotopes. Shielding dominated the relative activities for the same material in different locations. Vertical shielding ranged from essentially none (as in tray H-12) to moderate in trays C-3 and C-9 (about

1.7 g/cm²), mixed in tray G-12 (2.8 g/cm² for Ni and V and 8.0 g/cm² for Ta and In), and heavy (13 g/cm²) in the case of tray F-2. In trays G-12 and F-2, the heavier shielding was due to other activation samples or passive detectors placed on top of these samples. Trays C-3 and F-2 were most closely directed toward the peak of the anisotropic proton fluxes, but the large shielding in tray F-2 moderated this effect considerably. Some experiment trays have been modeled (Colborn and Armstrong, 1993) in sufficient detail to make quantitative comparisons with these measurements for trapped protons and cosmic rays. However, some qualitative observations can be made about the experimental results.

All long-lived radioisotopes with cross sections greater than 20 mb at energies above their respective reaction thresholds, and below about 200 MeV, were

detected in the nickel samples. Cross sections of radioisotope production for protons on nickel (Armstrong and Colborn, 1996) predict the largest yield for Co-57, although the cross sections increase for Co-58, Co-56 and Mn-54 and become stronger collectively than Co-57 above about 40 MeV. The appearance of these radionuclides were therefore expected in all samples. The relative strength of the activity of the nickel samples in tray C-3 probably reflected both the West-directed flux as well as the thin overlying shielding. As one progresses from Co-58 down to Mn-54, the effect becomes very pronounced. A small yield of Sc-46 was also seen in the C-3 and F-2 samples, for which the cross section only becomes important for proton energies of 100 MeV and above. The appearance of Sc-46 in the two trailing side samples and the larger yields of lighter nuclides in tray C-3 reflected the increased flux and/or harder spectrum of trapped protons from the West. The code predictions for the nickel samples with experimentally-determined cross sections (Armstrong and Colborn, 1992) underestimated the measured radionuclide yields by about 45% (Armstrong *et al.*, 1993), although the ratio of calculated to predicted activities is about the same for shorter-lived isotopes such as Co-56 and Co-58 as the longer half-life isotopes Mn-54 and Co-57. This strongly indicated that there was no large increase in radiation dose in the final months of the mission.

The radionuclides detected in the cobalt samples were similar to those of nickel as expected, with Co-57 also the dominant product for this target, although the strength of Co-58 also showed that the (p, pn) reaction and perhaps the (n, 2n) secondary reaction were strong contributors to the total yield. Unfortunately, an incomplete set of samples (no cobalt in trays F-2 or C-3) made it difficult to draw quantitative conclusions. Trays G-12 and C-9 gave very similar results consistent with the thinner vertical shielding in both trays though there was some disagreement between results from different laboratories.

The vanadium samples contained only one space-induced radionuclide (Sc-46) (it also contained substantial amounts of naturally-occurring uranium daughters) (Smith and Hurley, 1991). Its cross section is very uniform in energy above the Coulomb barrier (20–40 MeV) (Armstrong and Colborn, 1996), therefore protons produced Sc-46 with approximately equal probability at all depths. No sample was mounted in tray C-3, and tray F-2 was heavily shielded, so that these factors probably contributed to the relatively uniform activity in all four samples.

Indium radionuclide production is dominated by Sn-113 and In-114m. An interesting observation here was the higher yield of both these isotopes in tray F-2. This may have been an effect of the proton anisotropy together with neutron capture on In-113 (see below). Measurable yields of Ag-110 and Rh-102 showed that the activation samples were sensitive to significant

proton flux above 100 MeV, possibly cosmic rays, and were consistent with the appearance of Sc-46 in the nickel samples.

Tantalum presented a more difficult case to interpret because of the uncertainty in known experimental cross sections for this material. The lighter nuclides Lu-172 and Lu-173 appeared to reflect the proton anisotropy as shown in Table 3, but the heavier products did not. Armstrong predicted cross sections using YieldX and HETC (Armstrong and Colborn, 1996) for Hf-172 (decaying in equilibrium to Lu-172) and Lu-173 of 50–100 mb at trapped proton energies. Also, experimental results for Hf-175 (Laird, 1985) indicated cross sections of 70 mb at 60 MeV and 150 mb at 200 MeV. These cross sections are consistent with the activity levels of the radionuclides in Table 3.

3.3.1. *Neutron capture products.* Irradiation by trapped protons and cosmic ray primaries of a spacecraft the size of the LDEF was expected to yield a significant amount of secondary neutron flux. Most neutrons are made as secondary products from the proton-induced reactions, although a small percentage of the yield could be albedo flux off the atmosphere (see Armstrong and Colborn, 1992 and references therein). The higher energy neutrons (MeV) could have produced activation within the LDEF materials, but there are few long-lived gamma ray emitting nuclides made only by fast neutrons. For instance, the (n,p) reaction on Co-59 will produce Fe-59 ($T_{1/2} = 45$ d) with cross section $\cong 50$ mb at 14.5 MeV, but Fe-59 was not seen in the cobalt samples counted soon after retrieval.

Tantalum, indium, and cobalt have high thermal neutron capture cross sections (\sim barn, see radionuclides in boldface in Table 3). These materials are activated by very low energy thermal ($\approx .02$ eV) and epithermal neutrons that were moderated by low Z material on the LDEF. Only a few experiments carried significant amounts of plastic or organic compounds that efficiently slow energetic neutrons. Reeves *et al.* (1993) reported an enhanced Co-60 activity (neutron capture on Co-59) in the M0001 experiment, which contained plastic cosmic ray track detectors, relative to Co-60 activities in the other experiments. Similarly, the Ta-182 (neutron capture on Ta-181) was higher in the M0001 experiment and the P0004/6 experiments, the latter containing plastic detectors and organic material as well. A comparison of the neutron capture activities in the three samples is shown in Fig. 6, which represents a composite of data from LBL, PNL, and JSC from Table 3. The trends consistently indicated enhanced activity from capture products in the experiment trays containing moderator materials. The presence of high local thermal neutron flux therefore dominated over the different buildup and decay rates of these nuclides. It should be noted that In-114m probably included a significant fraction of proton-induced activation from In-115 (95.7% abundance). The metal samples in

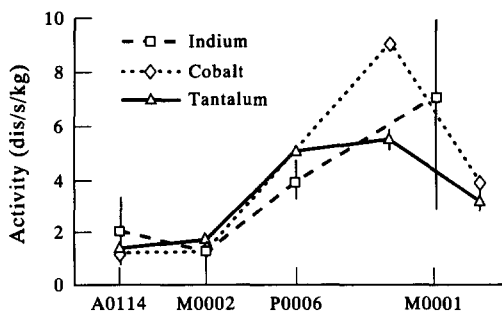


Fig. 6. Neutron capture activities for indium, cobalt, and tantalum metal samples from Exps. A0114, M0001, M0002, and P0006. Exp. M0001 had two samples of cobalt and tantalum, one each near the edge of the experiment tray and one near the center. Activities for each of the two sample pairs were extracted separately in this experiment. Exp. P0006 did not contain a cobalt sample.

Experiment M0001 were delivered for integration in the standard $2'' \times 2''$ geometry, but two smaller rectangular pieces ($2'' \times 3/4''$) were cut from the square plates for mounting on opposite sides of a sub-tray. The tantalum and cobalt rectangular plates were counted separately, and interestingly, showed a difference in activity from one side of the sub-tray and the other in Exp. M0001 (see Fig. 6). This appeared to be directly related to the amount of low Z material in proximity to the samples.

3.4. Steel trunnions

The steel trunnions (alloy 17-4PH) from the end support frame on the Earth end of the spacecraft (Fig. 1) were the first LDEF components acquired for analysis. The 17-4PH steel is approximately 75% iron with the remainder being nickel, chromium, copper, and other metals. The end faces of the cylindrical trunnions were roughly perpendicular to the flight vector, with one face each exposed to the east direction and one to the west (see Fig. 7). Samples were cut into two basic geometries. For bulk activity measurements, 0.5"-, 0.75"- and 1"-thick cylindrical sections were sliced along the axis of the trunnion (diameter 3.25"). Sections were designated as A, B, C, etc., where A denoted the trunnion end section farthest from the LDEF main structure. A second sample geometry was used to investigate the depth and azimuthal dependence of the activation. Three 2" long sections (D, G, and L) were further sliced along their central axis into concentric layers. The depth of the layered trunnion samples were determined by the distances in which protons are stopped in the material in 20 MeV steps between 20 and 120 MeV ($0-15.5 \text{ g/cm}^2$). The orientation of the trunnions allowed a section to be cut into four quadrants, each facing toward the Earth, space, north and south directions. Each quadrant was sliced into six layers to sample the activity versus radial depth. Layers 2-6 were also flattened to improve the detection efficiency. Layer 1

was not flattened to avoid damage to the trunnion surface. In section G a layer 7 ($\approx 23 \text{ g/cm}^2$) was also obtained from the trunnion core.

The most sensitive measurements of the trunnion sections revealed the presence of Mn-54, Sc-46, Cr-51, Co-56, Co-57 and Co-58 (Winn, 1992). The earliest measurements at MSFC (approximately 1 month after retrieval) also showed the presence of V-48. Mn-54 (half-life 312 d, 834 keV gamma ray) was expected to have the highest activity level in the trunnions based on the average energy of the trapped proton flux as well as the cross section for protons on iron. With an activity of 2-5 dis/s/kg, it was possible to map the Mn-54 activity throughout the trunnion volume. Directional and energy information about the activating particle fluxes could then be obtained. Figure 8 is a plot of the bulk Mn-54 activity in the two stainless steel trunnions from the Earth end of LDEF. The abscissa represents the distance along the trunnion axis measured from the end of the trunnion farthest from the spacecraft. Each point represents the average activity for one of the large cylindrical sections. The space-exposed end of the 'LH' trunnion was pointed West and offset to the North by the reported 8° yaw (Peters and Gregory, 1991), such that the axis of the trunnion was at an approximately 25° angle to the peak of the South Atlantic Anomaly proton flux angular distribution.

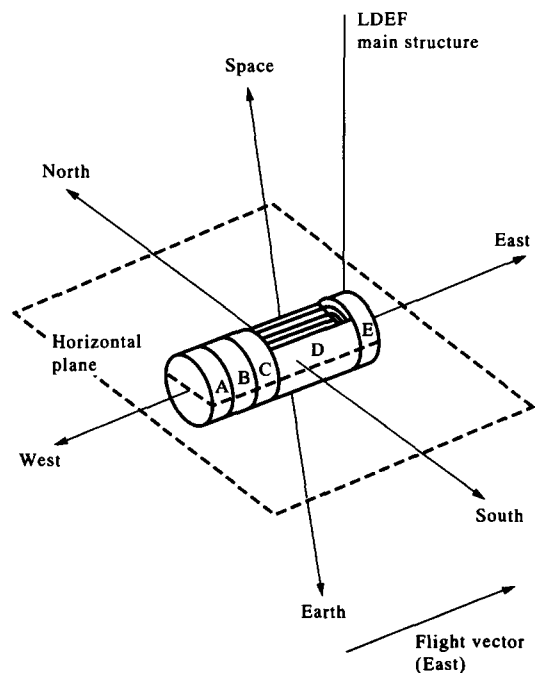


Fig. 7. Local geometry of the trailing (west) side trunnion. A, B, C, E, etc. identify cylindrical sections which were cut from the trunnion and counted individually. Sections D, G, and L were further processed into quadrants facing North, South, Space and Earth directions. The quartered sections were then cut into layers concentric with the center of the trunnion, as shown for section D, to examine the depth and directional dependence of the activity.

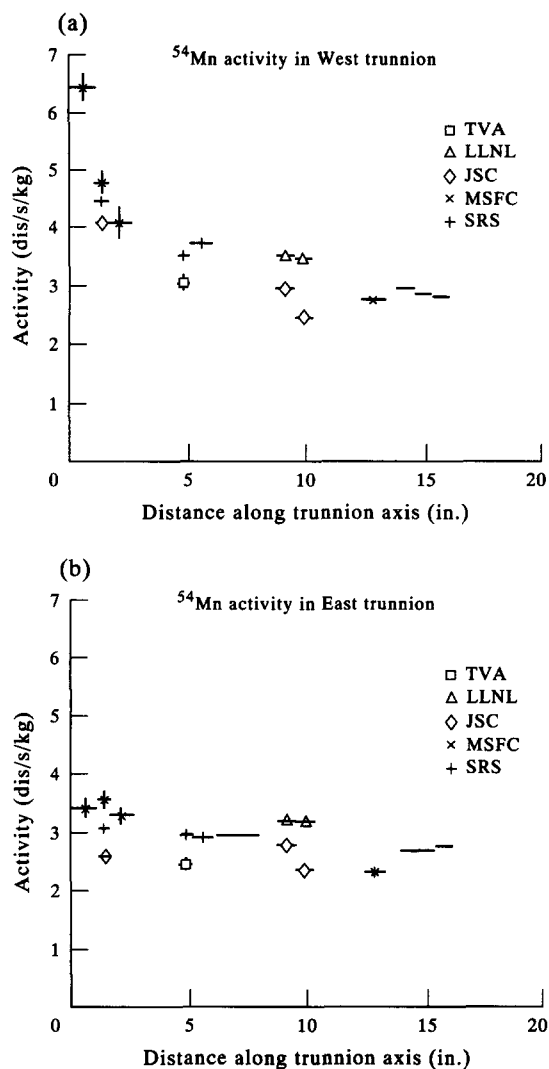


Fig. 8. Mn-54 activities in the end frame steel trunnions (East and West) as a function of distance along the trunnion axis. The origin of the horizontal axis represents the end of the trunnion farthest from the spacecraft.

As indicated in Fig. 8, several counting groups have analyzed the large cylindrical sections. These have a large self-attenuation of 834 keV gamma rays (as much as 50%) that must be accurately assessed to extract a specific activity. Although the statistical error for several day counts of the large trunnion pieces was small as shown in Fig. 8, systematic differences in the activity at the 20%–30% level were evidently present based on several measurements of the same sample (see activities measured at approximate distances of 1, 5, 9 and 10 inches along the axis of both East and West trunnions). The systematic differences also tended to be consistent between data sets. Both trunnions indicated a decreasing activity toward the spacecraft, with the SAA flux out of the West enhancing the activity considerably in the first two inches of the West trunnion. SAA protons are not

energetic enough to penetrate the entire length of the trunnion and would not explain the more gradual decrease that may be caused by shielding from the spacecraft.

Figure 9 shows the Mn-54 activity in trunnion layers from the West trunnion at a distance of approximately 7" from the end of the trunnion. The observed differences in the north, south, space and Earth directions were qualitatively similar to that in Moss and Reedy (1991), Smith and Hurley (1991), Harmon *et al.* (1992), and Winn (1991); Winn (1992). The higher sensitivity measurements indicated a very significant difference in flux between North and South. The SAA exposure produced an enhancement to the South (relative to North) caused by the southwesterly peak of the proton flux as expected. There was also a smaller space–Earth asymmetry, which was at least partially attributable to shielding by the spacecraft on the space side of the trunnion (Armstrong *et al.*, 1991). The variations in the shape of the activity versus depth curves shown in the upper part of the figure probably reflected the difference in the energy spectrum as a function of direction.

3.5. Steel screws from P0004/P0006 and experiment tray clamps

Steel canister screws (alloy A286) from experiment P0004/P0006 and a large number from the experiment tray clamps were obtained for activation measurement. These were generally too small to obtain measurements of good statistical accuracy from counting individual screws. The canister screws were grouped together by canister number (2–7), with two sets of screws from each canister: one from the cover plate (20 screws in the set); and one from the base plate (18 screws in the set). The tray clamp screws were also counted together to obtain maximum sensitivity to the radionuclides present.

Bulk counting of clamp screws by LLNL showed the presence Mn-54, Co-56, Co-57, Co-58, Na-22, and Be-7 (presumably surface deposition) with the Mn-54/Co-57 ratio being about 1.6–2.0 in the tray clamp screws, and a West/East ratio in the activities of 1.2–1.3. The Mn-54/Co-57 ratio appeared to be quite different from the steel in the trunnions Mn-54/Co-57 = 8–12) though efficiency corrections for odd-shaped samples with large attenuation are suspect. The presence of significant amounts of Na-22 may be related to low mass impurities or high-energy spallation reactions with cosmic rays. Results for the P0004/P0006 screws were not reported.

3.6. Titanium structural clips

Nine titanium structural clips (alloy 6AL-4V) (nominally 6% aluminum, 4% vanadium) were obtained from the internal frame of LDEF (approximate locations are shown in Fig. 1). The clips were mounted beneath the end intercostals, joining the intercostals to the longerons. Several groups (LBL, LANL and MSFC) reported Sc-46 and Na-22 in

these samples. Obtaining specific activities was possible although the geometry of these samples (slanted parallelepiped cross section) limited the accuracy of these measurements. Activities of 0.1–1 dis/s/kg for Na-22 and about 0.5–1.5 dis/s/kg for Sc-46 were reported (Smith and Hurley, 1991). The

6AL-4V alloy probably accounted largely for the Na-22 activity and for a part of the Sc-46 activity. Similar to the activation sub-experiment samples of vanadium, these samples contained significant amounts of naturally-occurring uranium daughter nuclides.

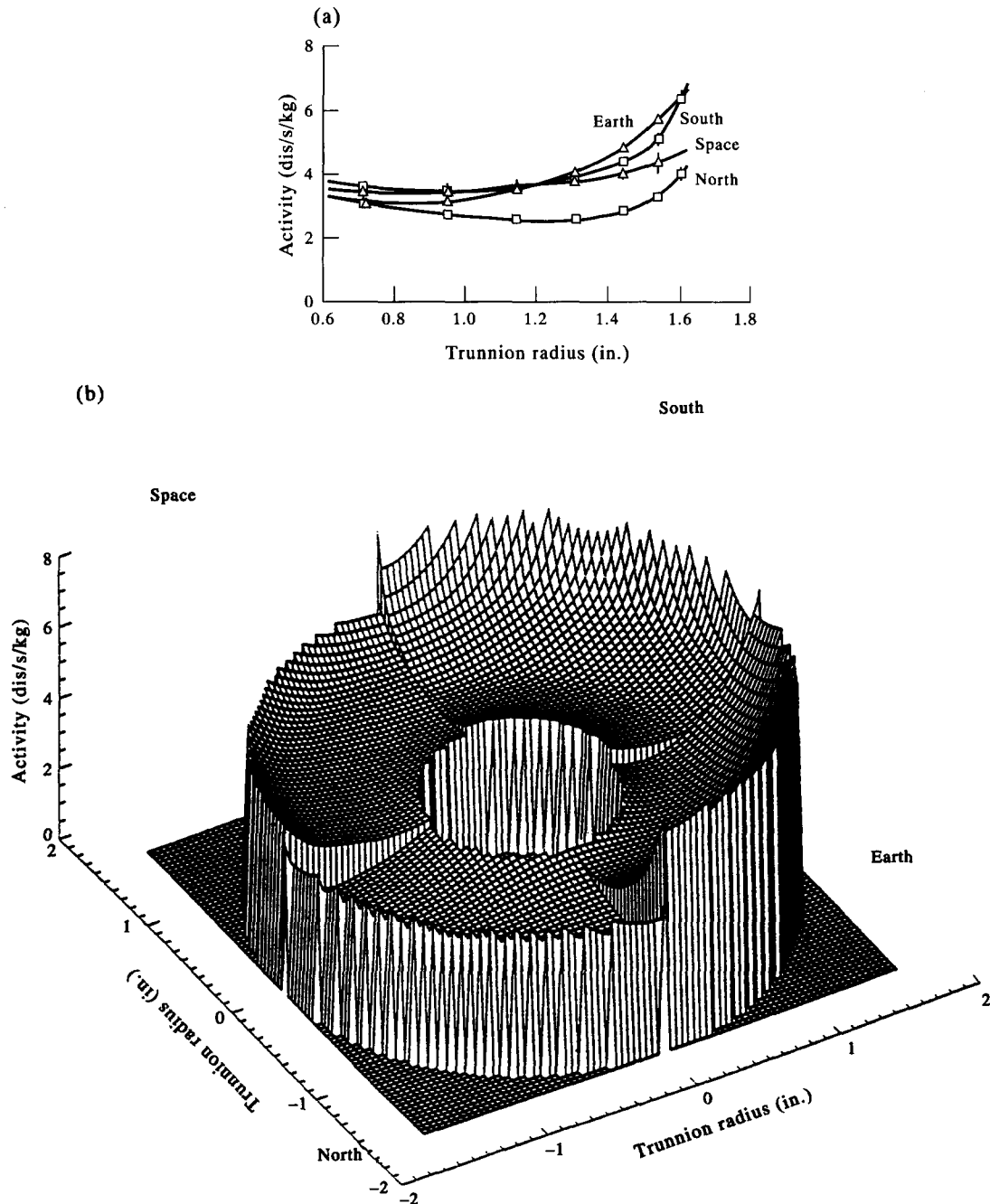


Fig. 9. Mn-54 activity as a function of radius and direction for thin steel layers taken from the West trunnion, section G. Top figure shows the activity profiles in the Earth, Space, North and South directions (most error bars are too small to be seen against data symbols). Continuous curves represent a spline fit to the data. The spline fits were then used to create the bottom figure, which is an approximate 2-D representation of the activity throughout the cylindrical section (0.6 in. radius core not analyzed). To accentuate the directional dependence of the activity, no smoothing was performed in the azimuthal direction.

3.7. Lead ballast plates

Lead was the highest atomic number ($Z = 82$) material obtained for activation measurement. The lead, used for stabilization of the spacecraft, was in the form of thin plates and arrived at MSFC six months after retrieval. The lead ballast and associated aluminum cover plates were mounted on the end frame I-beams from which material on rows 2 and 8 on the LDEF (see Fig. 1) were obtained. Representative $2'' \times 2''$ samples of lead ($1/8''$ to $1/4''$ thick) were cut from the ballast in both rows. Only Bi-207 at a very low activity was reported in the lead by LBL (Smith and Hurley, 1993) and JSC (Lindstrom, private communication). Activities were estimated to be about 0.1–0.3 dis/s/kg. In addition, LBL counted all lead samples that were available to them together in the ultra-low background facility at Oroville Dam to search for even weaker activities (Smith and Hurley, 1993). These results showed evidence of the radionuclides Mn-54 and Hf-172 among others. As a result of the relatively long half-life of Bi-207 ($T_{1/2} = 30.2$ y), and the lack of other radionuclides closer to the target atomic weight, it is not clear which, if any, of the detected radionuclides were produced from radiation exposure on orbit.

3.8. Other materials

A few small metal samples were obtained from other experiments (magnesium, silver, copper, niobium, molybdenum and germanium) several months after retrieval. Almost all had no detectable activity at the 0.5–1 dis/s/kg level or higher with the exceptions of magnesium (Na-22) and germanium (Zn-65). Olmez *et al.* (1991, 1993), reported results for larger samples of copper and zirconium which showed the presence of Co-58 and Y-88, respectively, consistent with production by trapped SAA protons.

4. CONCLUSION

The LDEF mission was unprecedented in its usefulness for passive radiation studies. No other spacecraft has allowed the combination of stabilized attitude and mission length for sensitive studies of the radiation environment in low Earth orbit. In particular, at the low altitudes (300–500 km) where many spacecraft are flown, the interaction of the upper atmosphere with the radiation belt is significant and complicates prediction of the radiation exposure. In order to carry out the study presented here, it was necessary to coordinate the measurements, corrections and reporting of data from a large number of laboratories using different counting and data acquisition systems. In the large part, this effort was very successful in determining very low specific activities (few dis/s/kg) in most materials to within reasonable systematic errors ($\approx 30\%$ or less). The LDEF results for induced

activity and dosimetry thus provide an important normalization for radiation environmental codes. As such, the LDEF results are relevant to current and future missions such as the Space Station, the Earth Observing System, and gamma ray astronomy satellites such as the Compton Observatory (Dyer *et al.*, 1989). LDEF dosimetric data have also been compared recently to similar data from the EURECA spacecraft (Benton and Frank, 1993), though detailed modeling remains to be completed.

The 5.8 y exposure of the LDEF showed clearly that the induced radioactivity was higher than expected from the modern radiation environmental codes for geomagnetically-trapped particles in use today. Detailed modeling, including both input fluxes from AP8MIN and AP8MAX codes applied in a realistic manner (Watts *et al.*, 1993a,b), combined with the best known accurate cross sections for long-lived radioisotopes (Armstrong and Colborn, 1992; Armstrong and Colborn, 1996 and references therein), yielded calculated activities that generally underestimated the observed induced radioactivity by a factor of 2. This was also the case for dosimetric measurements (Bourrieau, 1993; Frank *et al.*, 1993). In Exp. P0006, radiation predictions have been performed to cross-correlate results from thermoluminescent dosimetry data at various shielding depths with activation samples from the same tray (Armstrong *et al.*, 1993). Both induced activity and dosimetric data indicate the same deficiency in external trapped proton doses. Scoping calculations (Laird, 1985; Reedy *et al.*, 1993 see also, for example, Fig. 3) suggested that the effective fluence of trapped radiation of the LDEF mission was comparable to that from AP8MIN in the 450 km range or higher over the entire mission. The discrepancy with the more sophisticated modeling attempts will eventually need to be reconciled with our understanding of the behavior of the low Earth orbit radiation fields. The recent modification to the AP8 code for low altitude applications (Daly and Evans, 1993) improved the agreement with the LDEF data somewhat.

Qualitatively we found results that were consistent with trapped proton-induced reactions in the 20–200 MeV energy range, both in terms of radionuclides produced and directionality of the external fluxes. Using good quality cross-sections for proton-induced reactions on nickel, the predicted relative amounts of some isotopes (Armstrong *et al.*, 1993) agreed reasonably well with measured results for the nickel samples. This implied that the long-term time-dependence of the trapped protons fluxes was reasonably well-represented in the calculations. In some cases the presence of radionuclides with large neutron capture cross sections reflected the presence of nearby low- Z thermalizing materials. No radionuclides produced exclusively by fast neutrons (MeV or greater) were observed. The aluminum clamp plates provided the best example of

the flux anisotropy, but there were a number of other samples showing this effect. The depth profiles of the Mn-54 activity in steel suggested that both the intensity and spectrum of the activating particles were directionally-dependent.

The presence of Be-7 activity on the leading surfaces of the LDEF was a completely unexpected result and inconsistent with any particle-induced reaction with spacecraft materials. It was realized after measurements of both aluminum and steel components, and whole spacecraft measurements, that the Be-7 was being taken up from the upper atmosphere (≈ 300 km) as the spacecraft orbits the Earth. Even though Be-7 is known to be produced in the lower atmosphere around the Pfozter maximum (~ 18 km) and diffuses vertically (Benioff, 1956), the atmospheric concentration of Be-7 at the time of LDEF retrieval implied by the activity measurements was 1000 times more than would be expected based on a standard model atmosphere. Work is still in progress to determine the mechanism(s) involved in producing and/or transporting the Be-7 to orbital altitudes.

5. LDEF GAMMA-RAY DATA ARCHIVE

An archive of the gamma-ray data obtained by the counting laboratories has been established at the Space Science Laboratory at MSFC. This archive contains the gamma-ray data on 3.5" floppy disks in the format originally submitted to MSFC. In addition, the archive contains formal technical reports, data acquisition logs, computer analysis reports, and other associated information about the LDEF activation study. Some of the technical reports are available by request. To provide ready access to the spectral files without the requirement of the individual data acquisition software packages, two computer programs (Laird, 1996) have been supplied both in executable form for a 486-based personal computer and in the BASIC source code.

SpectraView (SV) is a simple gamma-ray display and analysis program developed to be used directly with the files submitted by the counting laboratories. Virtually all laboratories used different data acquisition systems. The most common was 4K (4096 channels), 4-byte data, ADCAM system at SRS and PNL while MSFC used an 4K, 4-byte ND66 analyzer, and JSC used an 8K, 4-byte Canberra S-100 system. LLNL submitted a 4K text-format data set, and LBL submitted a 4K, 4-byte MicroSampo format data set. SV allows the user to select which type spectra to view based on the extension on the file name. For instance, the PNL data has the extension PNW; MSFC data has ND6, etc. A list of the available files is given from which the user can choose a spectrum. A text file READMEL.DEF is available on one of the archived disks that gives more detail on the use of SV and on the spectral files.

SV will display a chosen gamma-ray spectrum and will allow the user to obtain the areas and energies of the displayed photopeaks. After the initial procedure for displaying a spectrum, various arrow and function keys allow for scanning the spectrum and for the determination of peak areas and energies. Since only an approximate energy calibration is available in the program, a recalibration using the data in the spectrum header or using known background peaks (i.e., 511 and 1460 keV) is advised. The procedure for such changes are found in READMEL.DEF.

The analysis of these gamma-ray spectra to get the activity per unit mass of material requires additional information beyond peak areas and energies. Relative to each spectrum the live time, the time from the start of counting, and the date of counting as well as the detector efficiency for a particular sample, the self-attenuation of photons by the sample, and the mass and shape of the sample must be known. The sample, the live time, the time and date of counting, and the energy calibration will usually be found in the header of the spectrum. HeaderView (HV) allows the user to read these headers. The header can be printed by using print screen or shift print screen. HV will read all of the files found on the archived disks except for text files which should be read with a DOS text editor. These text files are from LLNL and give the header and a listing of the spectra in a channel by channel format. Details about the LBL spectra must be obtained from the data logs stored with the archive at MSFC.

Acknowledgements—A number of individuals contributed along the way to the analysis of the LDEF induced radioactivity data. B. A. H. would like to thank Katherine Karr, Colleen Wilson, Michelle Flickinger, Fred Berry and John Horack for their efforts, and also members of the NASA/Langley Research Center LDEF Project Office for help with reasonably obscure details of the LDEF spacecraft. C. E. L. would also like to thank Wendy Ritter Ladd, Jonathan Fisher, Scott Mattingly, Scott Rucker, Martin Hackworth, Sundeep Arole, Robby Laird, Ricky Laird and Robert Kamau.

REFERENCES

- Armstrong T. W., Colborn B. L. and Watts J. W. Jr. (1991) Ionizing radiation calculations and comparisons with LDEF data, NASA CP-3134, pp. 347-360.
- Armstrong T. W. and Colborn B. L. (1992) Predictions of induced radioactivity for spacecraft in low Earth orbit. *Nucl. Tracks* **20**, 101-130.
- Armstrong T. W. and Colborn B. L. (1993) Radiation model predictions and validation using LDEF satellite data, NASA CP-3194, pp. 207-220.
- Armstrong T. W., Colborn B. L., Harmon B. A. and Laird C. E. (1993) Predictions of LDEF radioactivity and comparison with measurements, NASA CP-3275, pp. 203-216.
- Armstrong T. W., Colborn B. L., Harmon B. A. and Laird C. E. (1996) Prediction of the nuclear activation of materials on LDEF produced by the space radiation environment and comparison with flight measurements. *Radiat. Meas.* **26**, 765-777.

- Armstrong T. W. and Colborn B. L. (1996) Proton activation cross sections used in predicting LDEF satellite induced radioactivity, SAIC-TN-96030 report NASA Contract NAS8-39386, pp. 1-21 and appendix.
- Benioff P. A. (1956) Cosmic ray production rate and mean removal time of beryllium-7 from the atmosphere. *Phys. Rev.* **104**, 1122-1130.
- Benton E. V., Csige I., Frank A. L., Benton E. R., Frigo L. A., Parnell T. A., Watts J. and Harmon A. (1993) Absorbed dose and LET spectra measurements on LDEF, NASA CP-3275, pp. 135-148.
- Benton E. V. and Frank A. L. (1993) Preliminary results of radiation measurements on EURECA, NASA CP-3275, pp. 43-50.
- Bourrieau J. (1993) LDEF: Dosimetric measurement results (AO 138-7 experiment), NASA CP-3194, pp. 157-162.
- Clark L. G., Kinard W. H., Carter D. J. and Jones J. L., eds. (1984) The Long Duration Exposure Facility (LDEF) Mission 1 experiments, NASA SP-473, pp. 1-189.
- Colborn B. L. and Armstrong T. W. (1993) Development and application of a 3-D geometry/mass model for LDEF satellite ionizing radiation assessments, NASA CP-3194, pp. 195-206.
- Daly E.J. and Evans H.D.R. (1993) Problems in radiation environmental models at low altitude, ESA /ESTEC, Mem ESA/ESTEC/WMA/93-067/ED, April 23, 1993
- Dyer C. S., Truscott P. R., Sims A. J., Comber C. and Hammond N. D. A. (1989) Predictions of radiation backgrounds for GRO/OSSE, in *Proc. of Gamma Ray Observatory Workshop*, ed. by N. Johnson, (NASA Goddard, Greenbelt, unpublished), pp. 4, 521-528.
- Fishman G. J., Harmon B. A., Parnell T. A., Gregory J. C., Peters P., Haskins P. S., McKisson J. E., Ely D. W., Weisenberger A. G., Piercy R. B., Phillips G. W., King S. W., August R. A., Ritter J. C. and Cutchin J. H. (1991) Observation of ^7Be on the surface of the LDEF spacecraft. *Nature* **349**, 678.
- Frank A. L., Benton E. V., Armstrong T. W. and Colborn B. L. (1993) Absorbed dose measurements and predictions on LDEF, NASA CP-3194, pp. 163-170.
- Gregory J. C. (1996) Atmospheric radioactive isotopes at orbital altitudes. *Radiat. Meas.* **26**, 841-850.
- Gregory J. C., Fishman G. J., Harmon B. A. and Parnell T. A. (1991) The interactions of atmospheric cosmogenic radionuclides with spacecraft surfaces, NASA CP-3134, pp. 237-248.
- Gunnick R. and Niday J. B. (1972) Computerized quantitative analysis by gamma-ray spectrometry (Program GAMANAL), UCRL-51061, Vols. 1-4.
- Gunnick R. and Niday J. B. (1976) A working model for Ge(Li) detector counting efficiencies, Lawrence Livermore National Laboratory UCRL-77732, pp. 1-55.
- Harmon B. A., Fishman G. J., Parnell T. A., Benton E. V. and Frank A. L. (1992) LDEF radiation measurements: preliminary results. *Nucl. Tracks* **20**, 131-136.
- Harmon B. A. and Laird C. E. (1996) *Long Duration Exposure Facility induced radioactivity analysis Volume 2: activity results*, in preparation.
- Kinard W. H. and Martin G. D. (1991) Long Duration Exposure Facility (LDEF) space environments overview, NASA CP-3134, pp. 49-60.
- Laird C. E. (1985) Study of proton and neutron activation of metal samples in low Earth orbit, Eastern Kentucky University Final Technical Report, Contract NAS8-35180, pp. 1-12 and Appendices.
- Laird C. E. (1996) Study of activation of metal samples from LDEF-1 and Spacelab-2, Eastern Kentucky University Final Technical Report, Contract NASA H-13013D, pp. 1-147.
- Moss C. E. and Reedy R. C. (1991) *Measurements of induced radioactivity in some LDEF samples*, pp. 271-285.
- Olmez I., Burns F. and Sagalyn P. L. (1991) Charged particle activation studies on the surface of LDEF spacecraft, NASA CP-3134, pp. 255-256.
- Olmez I., Burns F. and Sagalyn P. L. (1993) Charged particle activation studies on the surface of LDEF spacecraft, NASA CP-3194, pp. 107-110.
- Parnell T. A. (1991) Summary of ionizing radiation analysis on the Long Duration Exposure Facility, NASA CP-3134, pp. 199-212.
- Peters P. N. and Gregory J. C. (1991) Pinhole cameras as sensors for atomic oxygen in orbit; application to attitude determination of the LDEF, NASA CP-3134, pp. 61-68.
- Petty G. W. (1991) Equilibrium profiles of atomic ^7Be and ^{10}Be in the atmosphere above 100 km. *Geophys. Res. Lett.* **18**, 1687-1690.
- Phillips G. W. and Marlow K. W. (1976) Automatic analysis of gamma-ray spectra from germanium detectors. *Nucl. Inst. and Meth.* **137**, 525-536.
- Phillips G. W., King S. E., August R. A., Ritter J. C., Cutchin J. H., Haskins P. S., McKisson J. E., Ely D. W., Weisenberger A. G., Piercy R. B. and Dybler T. (1991a) Gamma radiation survey of the LDEF spacecraft, NASA CP-3134, pp. 225-236.
- Phillips G. W., King S. E., August R. A., Ritter J. C., Cutchin J. H., Haskins P. S., McKisson J. E., Ely D. W., Weisenberger A. G., Piercy R. B. and Dybler T. (1991b) Discovery of Be-7 accretion in low Earth orbit. *Adv. in Astron. Sci.* **91-076**, 575-583.
- Reedy R. C., Moss C. E., Bobias S. G. and Masarik J. (1993) Radioactivities induced in some LDEF samples, NASA CP-3194, pp. 87-96.
- Reeves J. H., Arthur R. J. and Brodzinski R. L. (1993) Sensitivity of LDEF foil analyses using ultra-low background germanium vs. large NaI (TI) multidimensional spectrometers, NASA CP-3194, pp. 79-86.
- Rich F. J., Michael I., Fishman G. J., Segalyn P. L., McNulty P. J., Rao Y. V. and Laird C. E. (1984) Trapped-proton energy spectrum determination M0002-1, in The Long Duration Exposure Facility (LDEF) Mission 1 experiments, (eds. Clark L. G., Kinane W. H., Carter D. J. and Jones J. L.) NASA SP-473, pp. 109-112. Samples were also contained in Exps. A0114 (pp. 14-19), M0001 (pp. 105-108) and P0006 (pp. 115-116).
- Routti J. T. and Prussin S. G. (1969) Photopeak method for the computer analysis of gamma-ray spectra from semiconductor detectors. *Nucl. Inst. and Meth.* **72**, 125-142.
- Sawyer D. M. and Vette J. I. (1976) AP-8 Trapped Proton Environmental for Solar Maximum and Solar Minimum, National Science Data Center, Goddard Space Flight Center, NSSDC/WDC-A-R and S 76-06.
- Smith A. R. and Hurley D. L. (1991) Radioactivities of Long Duration Exposure Facility (LDEF) materials: baggage and bonanzas, NASA CP-3134, pp. 257-270.
- Smith A. R. and Hurley D. L. (1993) Doing photons with Merlin II at Oroville, NASA CP-3275, pp. 189-198.
- Watts J. W., Armstrong T. W. and Colborn B. L. (1993a) Revised predictions of LDEF Exposure to Trapped Protons, NASA CP-3194, pp. 137-146.
- Watts J. W., Armstrong T. W. and Colborn B. L. (1993b) Status of LDEF Radiation Modeling, NASA CP-3275, pp. 217-226.
- Watts J. W., Armstrong T. W. and Colborn B. L. (1996) Predictions of LDEF exposure to the ionizing radiation environment. *Radiat. Meas.* **26**, 893-899.
- Watts J. W., Parnell T. A. and Heckman H. H. (1989) Approximate angular distributions and spectra for geomagnetically trapped protons in low-Earth orbit.

AIP Conference Proceedings 186, High Energy Radiation Background in Space (eds A. C. Rester and J. I. Trombka), pp. 75–85. AIP, New York.

Winn, W. G. (1991) Gamma-ray spectrometry of LDEF samples at SRL, NASA CP-3134, pp. 287–300.

Winn, W. G. (1992) Gamma-ray spectrometry of LDEF

samples, Westinghouse Savannah River WSRC-RD-91-16, pp. 1–26., App. A–C.

Winn, W. G. (1993) Gamma-ray spectrometry of LDEF samples – results of 1992 analyses, Westinghouse Savannah River WSRC-TR-93-430, pp. 1–9., App. A–C.